A System Model for Low-Level Approach

W. A. JOHNSON* AND D. T. MCRUER†
Systems Technology Inc., Hawthorne, Calif.

To maintain adequate safety levels when the minimum decision height is lowered from 200 ft (Category I) to 100 ft (Category II) requires an improvement in final approach guidance accuracy. An assessment of this guidance accuracy can be made by defining a successful approach as one in which the airplane deviations are within prescribed limits. Based on this simple definition, a model has been developed which provides, as its primary output, the probability of a successful Category II approach. Typical results are given for two example systems subjected to random gusts and deterministic wind shear. The major use of the model is to assess changes in the basic airframe, controller, inputs, or approach window dimensions, and to serve as one basis for the comparison of competing system mechanizations.

Introduction

THIS paper describes a system model for analyzing Category II approaches and presents examples of its application. Although the model considers both the longitudinal and lateral situations, only the longitudinal will be discussed in any detail here.

The primary purpose of the approach system model developed in this paper is to establish a structure containing the system elements, command inputs, disturbances, and their interactions in an analytical framework so that the relative effects of changes in the various system elements on precision of control and available margins of safety can be estimated. The model is intended to provide insight for the design and integration of suitable autopilot, display, and navigation elements; and to assess the interaction of such elements with the pilot/co-pilot.

Table 1 Approach outcomes

Basic outcome	Associated performance measures
Successful landing	Dispersions at decision height and/or reference position and at touchdown
Successful missed approach	Dispersions at decision height
Accident	
Short landing	Longitudinal touchdown location
Hard landing	Sink rate at touchdown
Overrun runway during rollout	Airspeed and altitude errors at reference position
Land off side of runway	Lateral touchdown location
Drag a wing tip or engine pod during landing	Bank angle at touchdown
Land with excessive misalignment angle (putting side loads on landing gear)	Side velocity at touchdown
Run off side of runway during rollout	Lateral displacement deviations during rollout

The approach model consists of three basic elements, a) a dynamic block diagram (Fig. 1), b) approach outcome definitions (Table 1), and c) an outcome probability tree (Fig. 2). The dynamic block diagram includes the controlled element as well as the control loops used to make up the closed-loop system, the approach-outcome definitions indicate the approach outcomes that are considered, and the outcome probability tree indicates how the various approach outcomes might be represented quantitatively.

A key aspect of the model is the probability tree, which represents its set of outputs. From Fig. 2 it is easy to visualize, conceptually, how a model might be constructed to give all the various approach outcome probabilities as outputs. However, because accident probabilities are extremely small quantities, it is more meaningful to concentrate on the probability of a missed approach, and to consider this as a primary measure of a system's adequacy. This is supported by existing information indicating that at the Category II-B level the missed approach rate may possibly be as high as 40%.[1]

An overview of the steps required in using the model can be described briefly as follows. The functions to be performed during an approach, the mechanization of the controller, and the vehicle dynamics are first defined (e.g., glide slope and localizer tracking via a coupled autopilot in a DC-8). Then the inputs to the system are defined (such as gust disturbances and beam noise), and performance metrics are calculated (e.g., rms altitude deviations from the glide slope beam). Finally, with performance metrics available, critical limits on approach outcomes can be defined, and approach

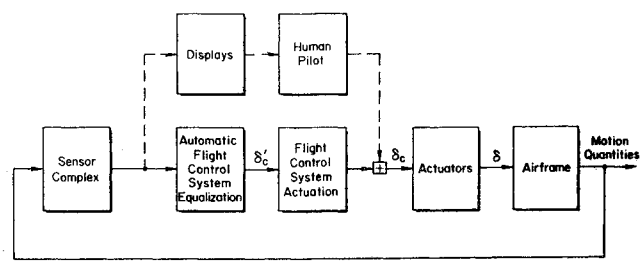

Fig. 1 Dynamic block diagram (longitudinal).

Presented as Paper 70-1034 at the AIAA Guidance, Control and Flight Mechanics Conference, Santa Barbara, Calif., August 17–19, 1970; submitted September 2, 1970; revision received May 19, 1971. This paper includes research efforts supported by the NASA Ames Research Center, Moffett Field, Calif., under Contract NAS2-4892.

Index category: Aircraft Landing Dynamics.

* Senior Research Engineer. Member AIAA.

† President and Technical Director. Associate Fellow AIAA.

Table 2 Control equations and functions performed by the example systems

	Function	System A	System C
Attitude control and regulation	Short-period attitude stiffness	$\theta \rightarrow \delta_e$ in short-period frequency range	
	Short-period damping; path-loop bandwidth extension capability	$\dot{\theta} \rightarrow \delta_e$ in short-period frequency range	
	Short-term w_g windproofing	High-frequency θ washout	No θ washout
Path control and regulation	Higher-order path following Trim Windproofing (w_g step)	$\int dt \rightarrow \delta_e$	
	Path acquisition and stiffness Windproofing (u_g step, w_g pulse)	$d \rightarrow \delta_e$	
	Path damping	$\dot{h} \rightarrow \delta_e$	$\theta \rightarrow \delta_e$
	Control equations	$-\delta_{ec} = [(K_{\bar{d}} + K_d s)/s(T_f s + 1)]d + K_{\dot{h}}\dot{h} + \{K_\theta s/[s + (1/T_{wo})]\}\theta + K_{\dot{\theta}}\dot{\theta}$	$-\delta_{ec} = K_d d/(T_f s + 1) + K_\theta \theta$

outcome probabilities can be computed. By considering the distribution of gust levels, and integrating over all gust levels, an over-all "average" probability is obtained. Thus, the end result is a set of performance metrics and approach outcome probabilities for a specific system mechanization subjected to a given input and disturbance environment. Direct comparisons of systems can be made simply by going through the analysis steps for each competing system mechanization with a standardized set of inputs. To illustrate the process, two example systems are described and compared. These two systems are both automatic, but with different feedbacks to the autopilot.

The basic requirements for an autopilot derive from guidance, control, and regulation considerations. A summary of various closed-loop characteristics and the feedbacks used to achieve them is given in Table 2 (a detailed development can be found in Ref. 4), while block diagrams for each system are given in Figs. 3 and 4.

System Inputs

For the purposes of evaluating and comparing systems, it is necessary to subject them to an appropriate set of inputs. To cover a variety of situations, three types of input disturbances which are commonly encountered during an approach were considered; 1) random gusts, 2) deterministic gusts, and 3) ILS beam noise.

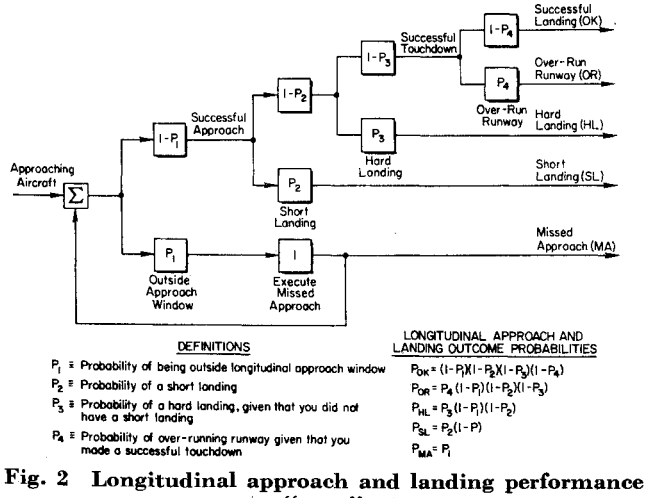

Fig. 2 Longitudinal approach and landing performance "tree."

Random Gusts

The random gusts considered here are defined by components along all three axes. Because analysis of measured gust data has revealed nearly Gaussian distributions, the assumption of zero-mean Gaussian distributions for the random gusts will be made.

Considerable gust data from numerous sources has been integrated to produce a gust model appropriate for design analysis purposes.[2] The basic form is defined by three power spectral densities which relate normalized gust intensities to spatial frequency. In terms of temporal frequency these spectra are given by

$$\Phi_{u_g}(\omega) = \sigma_{u_g}^2 \frac{2L_u}{\pi U_0} \frac{1}{1 + (L_u\omega/U_0)^2} \quad (1)$$

$$\Phi_{v_g}(\omega) = \sigma_{v_g}^2 \frac{L_v}{\pi U_0} \frac{1 + 3(L_v\omega/U_0)^2}{[1 + (L_v\omega/U_0)^2]^2} \quad (2)$$

$$\Phi_{w_g}(\omega) = \sigma_{w_g}^2 \frac{L_w}{\pi U_0} \frac{1 + 3(L_w\omega/U_0)^2}{[1 + (L_w\omega/U_0)^2]^2} \quad (3)$$

where L_u, L_v, L_w = scale length (ft), U_0 = aircraft's mean speed with respect to the air mass (fps), ω = frequency (rad/sec), σ = standard deviation.

Conforming to the stipulations of Ref. 2, the random turbulent velocity components have been assumed to be uncorrelated. Although this assumption is fully justified for clear air turbulence at high altitudes, it is not strictly true at low altitudes because of prevailing anisotropy in the boundary layer. However, Ref. 2 mentions that at low altitudes the cross-correlations between the gust components are

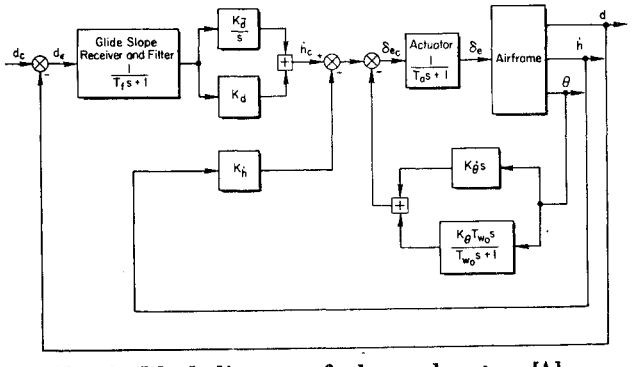

Fig. 3 Block diagram of advanced system [A].

weak, and may therefore be disregarded. Consequently, the analysis can be carried out using the three components of the gust model separately.

This gust model represents stationary, random gusts as stationary processes. However, the gusts actually *encountered* by a *descending* airplane are nonstationary due to the altitude dependence of the gust characteristics. Further, because the break points in the analytic expressions for the gust-power spectra are nonlinear functions of altitude, the spectral characteristics of the gusts encountered by a descending airplane are nonlinear functions of time. However, in spite of these complicating factors, reasonably accurate performance calculations can still be made quite simply, as will be explained below.

The computation of the rms output of a linear system to a stationary random input is well known and straightforward. All that is needed is a closed-loop system transfer function and a spectral representation of the input. (The pertinent closed-loop transfer functions for our example cases are given in the Appendix, with the details available in Ref. 4.) Figure 5 shows the required calculations, where c might represent altitude, and i might represent a vertical gust (for example). Implicit in such calculations is the assumption that the system has been operating for a sufficiently long (theoretically infinite) time so that all transients have died out. For practical purposes, however, all that is really required is that steady-state conditions have been reached, i.e., that the system has been operating on the stationary input long enough for the output to become approximately stationary. The time required for this to occur depends on the system dynamics. For our model airplane plus controller, this time is relatively short; of the order of 5 sec (based on the settling time for step inputs). Thus, although the mathematics requires a stationary input to be applied to a system for an infinite time, only the most recent 10 sec (or so) of input has any appreciable effect on the airplane's current condition. This observation has the happy consequence that the complete nonstationary gust input to the descending airplane is not required to estimate the airplane dispersions at the Category II decision height of 100 ft altitude. Instead, only the gust characteristics corresponding to the last 5–10 sec preceding the altitude of interest need be considered. Because the airplane sink rate is about 10 fps, 5–10 sec corresponds to about 50–100 ft altitude change. For such a small altitude change, the altitude-dependent gust parameters do not change very much during the time interval of interest. Therefore, the required "short-time" gust model is essentially a stationary input which is closely approximated by the gust model components evaluated at an altitude of 100 ft.

The probability of occurrence of the gust intensities σ_{w_g} at various altitudes is represented by $P(\sigma_{w_g})$, defined as the exceedance probability

$$P(\sigma_{w_g}) = P_1 \hat{P}(\sigma_{w_g}) \tag{4}$$

where P_1 *is the probability of occurence of clear-air turbulence, and* $\hat{P}(\sigma_{w_g})$ *is the probability of equalling or exceeding a given magnitude of* σ_{w_g} *once clear-air turbulence is encountered.*

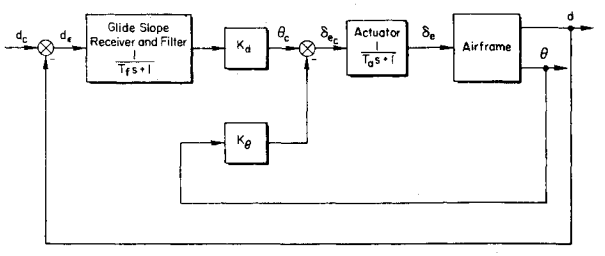

Fig. 4 Block diagram of conventional system [C].

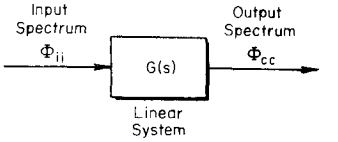

Fig. 5 Computation of rms output from input spectrum and closed-loop system transfer function.

$$\Phi_{cc}(\omega) = |G(j\omega)|^2 \Phi_{ii}(\omega)$$

$$\sigma_c^2 = \int_0^\infty \Phi_{cc}(\omega) d\omega$$

Reference 2 gives the probability of occurrence of clear-air turbulence, P_1, at 100 ft altitude as 0.8, and the probability $\hat{P}(\sigma_{w_g})$ of equalling or exceeding a given σ_{w_g} as

$$\hat{P}(\sigma_{w_g}) = \exp\left(-\frac{1}{2}\frac{\sigma_{w_g}^2}{5.29\ \text{ft}^2/\text{sec}^2}\right) \tag{5}$$

Deterministic Gusts—Wind Shears

Although horizontal wind shear near the ground is a relatively common phenomenon, it is still not fully understood. This is due, in part, to the paucity of shear measurements. As a result, such things as probability of encounter, and distribution of shear magnitudes at various altitudes are not presently known.

However, taking into consideration available data and information on shear, standard shear inputs were selected. For our calculations, wind shear is simulated by introducing an altitude dependent steady wind. For the headwind component, the variation with altitude starts at 200 ft and is linear down to an altitude of 100 ft at a rate of 4 knots/100 ft. Although this magnitude may be considered somewhat arbitrary, it is representative of actual measured shears, and is consistent with current thinking in the industry.

ILS Beam Noise

The effects of beam noise, for both the localizer and glide slope signals, can be determined by exciting the system with beam noise inputs. Glide slope noise measurements at LaGuardia (made by the FAA in January 1967) have been reduced at STI. Although this is not a Category II beam, the rms noise level of the beam from the outer marker down to the middle marker happens to just meet Category II criteria. Thus, it is considered representative of actual Category II beam characteristics. The PSD plot pertinent to this segment of the beam is the one used here, and is given in Fig. 6 along with a data fit by a simple analytical expression.

A short-time stationarity argument similar to that used earlier for random gusts can also be applied to beam noise. That is, even though the noise properties may be range-dependent, they are relatively stationary over intervals of the order of airplane/system settling times, and can therefore be treated as stationary inputs.

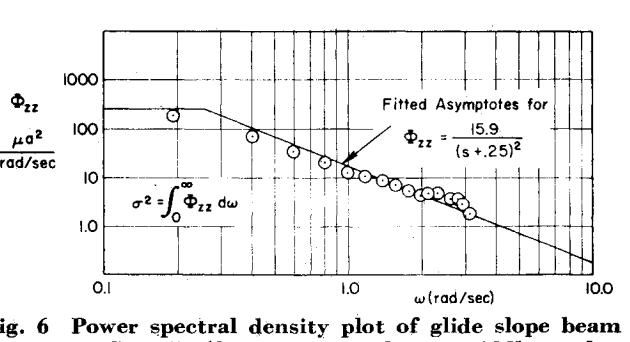

Fig. 6 Power spectral density plot of glide slope beam noise at LaGuardia (from outer marker to middle marker at low tide)—rms level is 10 μa.

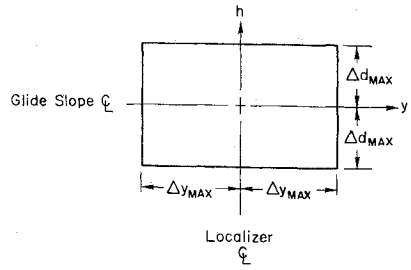

Fig. 7 Category II approach window (at 100 ft altitude) for altitude and lateral displacement deviations.

Definition of Approach Window

The purpose of an approach window is to define the critical limits for continuing an approach beyond the decision height. The approach window is defined in terms of three parameters: altitude, lateral displacement, and airspeed. Figure 7 shows a spatial Category II window that the airplane should be within at the 100 ft decision height (in addition to maintaining airspeed within the airspeed window).

The values of the variables that define a nominal longitudinal approach window are: $\Delta d_{\max} = 12$ ft and $\Delta u_{\max} = 5$ knots. The Δd limit corresponds to 1 dot of glide slope error at 100 ft altitude. This is a limit the FAA quotes for Category II operation in Ref. 3. The airspeed limit was also selected on the basis of FAA criteria.[3] At this point we might note that a steady 12 ft altitude error on a 2.8° glide path corresponds to a longitudinal touchdown error of 246 ft, which still puts the airplane well within the acceptable landing zone.

Example Calculations

By making the assumptions of stationarity and normal (Gaussian) distributions for the variables we can compute the means and rms deviations of the pertinent variables from their mean values (via the inputs and equations of motion). Then the probability density distribution plots, such as those shown in Fig. 8, can be used to determine the over-all approach success probability.

The calculations of these means and rms deviations are quite simple to perform. The mean values of the variables are computed from deterministic inputs, and the rms values from zero-mean Gaussian (random) inputs, as indicated schematically in Fig. 9. For longitudinal missed approach calculations, only d (glide slope deviation) and u calculations are required. The total rms values of d and u are found by adding the contributions due to each input on an RSS (a square root of summed squares) basis. Thus, for random

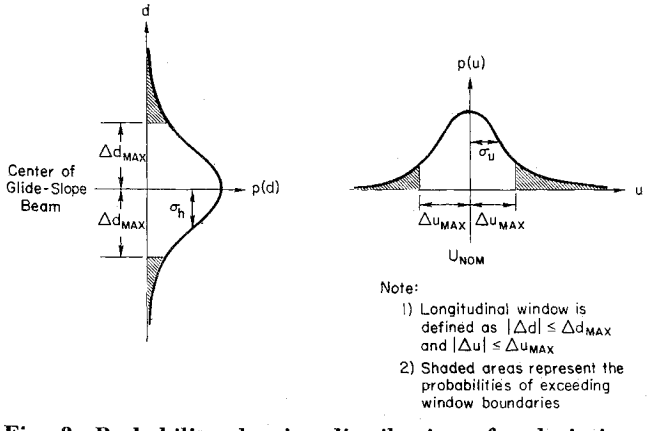

Fig. 8 Probability density distributions for deviations from the glide slope beam and nominal velocity (shown for zero-mean inputs).

Table 3 Category II approach success probabilities

System	Random u_g and w_g and glide slope noise		Random u_g and w_g, glide slope noise and u_g shear = 4 kt/100 ft for last 100 ft before window	
	P_{SA} for $\sigma_{w_g} = 4$ fps	Over-all P_{SA}	P_{SA} for $\sigma_{w_g} = 4$ fps[a]	Over-all P_{SA}
A	0.965	0.976	0.78	0.90
C	0.63	0.83	0.49	0.74

[a] This gust level occurs about 18% of the time (Ref. 2).

gusts and glide slope noise inputs,

$$\sigma_d = (\sigma_{d_1}{}^2\sigma_{w_g}{}^2 + \sigma_{d_2}{}^2\sigma_{u_g}{}^2 + \sigma_{d_{gs}}{}^2)^{1/2} \quad (6)$$

and

$$\sigma_u = (\sigma_{u_1}{}^2\sigma_{w_g}{}^2 + \sigma_{u_2}{}^2\sigma_{u_g}{}^2 + \sigma_{u_{gs}}{}^2)^{1/2} \quad (7)$$

Equations (6) and (7) can be simplified by making use of the relation between σ_{w_g} and σ_{u_g} at an altitude of 100 ft.[2] That is,

$$\sigma_{u_g} = 2.59\sigma_{w_g} \quad (8)$$

Thus, using Eq. (8) and the appropriate values for System A, Eqs. (6) and (7) become,

$$\sigma_d(\text{ft}) = (1.62\sigma_{w_g}{}^2 + 3.30)^{1/2} \quad (9)$$

$$\sigma_u(\text{fps}) = (0.750\sigma_{w_g}{}^2 + 0.058)^{1/2} \quad (10)$$

Figure 10 is a plot of these last two relations (for System A) and shows that the glide slope noise contribution is negligible for σ_{w_g} greater than about 2 fps.

At this point σ_{w_g} can be used as an independent variable to obtain values for σ_d and σ_u, leading to the probability of a successful approach ($P_{SA} = 1 - P_{MA}$) as a function of σ_{w_g}. Such a relation is presented in Fig. 11 for System A, where it can be seen that the probability of a successful approach drops below 0.5 when σ_{w_g} exceeds about 9 fps.

Similar probabilities could be computed for alternative systems, and comparison could be made. However, these probabilities are conditional probabilities because they are based on the assumption of given gust levels. Therefore, a further consideration will be introduced here to account for the distribution of gust levels. This will enable an over-all probability of a successful approach to be made; one that will be more meaningful in terms of long-time nationwide averages.

This over-all probability is preferred over the conditional probability as a performance metric for comparison of systems because it makes possible a quantitative assessment of relative system merit. That is, a dollars and cents value of one

Table 4 DC-8 parameters for landing approach configuration

Geometry and inertial properties			Stability derivatives	
h	(ft)	0	X_u (1/sec)	−0.0373
M	(−)	0.204	X_w (1/sec)	0.136
V_{T_0}	(fps)	228.	X_{δ_e} (fps²/rad)	0
γ_0	(deg)	−2.8°	Z_u (1/sec)	−0.283
q	(lb/ft²)	61.8	Z_w (1/sec)	−0.750
S	(ft²)	2758.	Z_{δ_e} (fps²/rad)	−9.25
b	(ft)	142.4	M_u (1/sec-ft)	0
c	(ft)	22.16	M_w (1/sec-ft)	−0.00461
W	(lb)	180,000	$M_{\dot{w}}$ (1/ft)	−0.00085
m	(slugs)	5,580	M_q (1/sec)	−0.594
I_x	(slug-ft²)	3.2×10^6	M_{δ_e} (1/sec²)	−0.923
X_{CG}	(% c)	25.2	M_α (1/sec²)	−1.05
δ_{F_0}	(deg)	50	$M_{\dot{\alpha}}$ (1/sec)	−0.1936

Table 5 Summary of control system constants

	Units	System A	System C
K_θ	...	−2	−3.652
$K_{\dot\theta}$	sec	−2	0
$K_{\bar a}$	rad/ft-sec	−0.000768	0
K_d	rad/ft	−0.00867	−0.00514
$K_{\dot h}$	rad/fps	−0.0256	0
$1/T_{WO}$	1/sec	0.7	...
$1/T_a$	1/sec	15	15
$1/T_f$	1/sec	2	2

system over another can be made if an over-all approach success probability is known; as opposed to knowing only that one system will result in 10% more missed approaches than another when σ_{w_g} is 5 fps, and 17% more missed approaches when σ_{w_g} is 3 fps. The key point here is that the ratio, as well as the difference, of missed approach probabilities for two different systems is a function of the gust level encountered. Therefore, the relative value of one system over another will depend on the gust level encountered.

The distribution of gust levels can be taken into consideration, via

$$P_{MA} = 0.2P(MA|\sigma_{w_g} = 0) + 0.8\int_0^\infty P(MA|\sigma_{w_g})p(\sigma_{w_g})d\sigma_{w_g} \tag{11}$$

where P_{MA} is the over-all probability of a missed approach; $P(MA|\sigma_{w_g})$ is the conditional probability of a missed approach and is a function of σ_{w_g} (see discussion leading to Fig. 11); $p(\sigma_{w_g})$ is the probability density distribution of σ_{w_g}, given that clear-air turbulence is encountened (see next paragraph); and 0.8 is the probability of encountering clear-air turbulence at an altitude of 100 ft.[2]

The function $p(\sigma_{w_g})$ is determined from $\hat P(\sigma_{w_g})$, given earlier, by differentiation. Thus,

$$p(\sigma_{w_g}) = (\sigma_{w_g}/5.29)e^{-(1/2)(\sigma_{w_g}/2.3)^2} \tag{12}$$

With these equations it is now a simple matter to compute the over-all probability of a missed approach (or a successful approach). For the example case of System A with random u_{gust}, w_{gust}, and glide slope noise, the over-all probability of a successful approach is 0.976. However, by adding a horizontal wind shear of 4 knots per 100 ft from 200 ft to 100 ft the probability of a successful approach drops to 0.90. These numbers are summarized in Table 3 which shows a comparison of approach success probabilities for two sets of inputs applied to both example systems. Also, included in the table, is a column giving the probability of a successful approach for a gust level that is equalled or exceeded about 18% of the time. This column was presented to show that the missed-approach rate for a moderately gusty condition is considerably greater than the over-all average missed-approach rate.

Table 6 Closed-loop transfer functions for System A[a]

$$\frac{d}{u_g} = \frac{-0.283(0)(0)(0.174)(2.0)(12.918)[0.767,2.215]}{(0.036)(0.123)(0.582)(2.462)(13.232)[0.657,0.699][0.673,1.428]}$$

$$\frac{d}{w_g} = \frac{-0.75(0)(2.0)(13.75)[0.464,0.103][0.936,2.018]}{(0.036)(0.123)(0.582)(2.462)(13.232)[0.657,0.699][0.673,1.428]}$$

$$\frac{d}{d_{\text{command}}} = \frac{-2.406(0.035)(0.089)(0.7)(-3.606)(4.396)}{(0.036)(0.123)(0.582)(2.462)(13.232)[0.657,0.699][0.673,1.428]}$$

$$\frac{u}{u_g} = \frac{-0.0373(0.136)(1.596)(2.777)(13.261)[0.5,0.276][0.58,1.918]}{(0.036)(0.123)(0.582)(2.462)(13.232)[0.657,0.699][0.673,1.428]}$$

$$\frac{u}{w_g} = \frac{-0.136(0.153)(0.215)(2.409)(13.262)[-0.082,1.023][0.872,1.492]}{(0.036)(0.123)(0.582)(2.462)(13.232)[0.657,0.699][0.673,1.428]}$$

$$\frac{u}{d_{\text{command}}} = \frac{0.3272(0)(0.089)(0.7)(-4.082)(4.03)}{(0.036)(0.123)(0.582)(2.462)(13.232)[0.657,0.699][0.673,1.428]}$$

[a] The shorthand notation used here is defined as follows

$K(s + a)/(s + b)[s^2 + 2\zeta\omega s + \omega^2]$ becomes $K(a)/(b)[\zeta,\omega]$

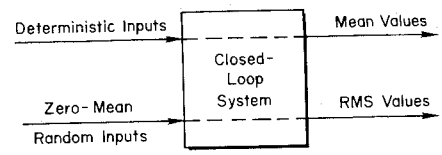

Fig. 9 Schematic representation of effects of deterministic and random inputs.

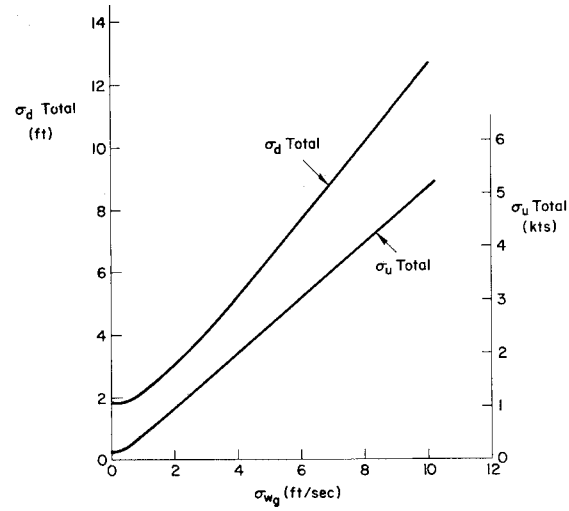

Fig. 10 σ_d(total) and σ_u(total) as function of the w_g-gust intensity (for System A).

A comparison of the approach success probabilities shows that System A is considerably better than System C. System A's clear superiority was certainly no surprise. In fact, it was an expected result, because System A was designed to be an advanced autopilot.

These example calculations illustrate a major use of the model presented herein, i.e., as a practical and efficient means for comparing systems on the basis of approach success probabilities. However, the over-all approach success probability is sensitive not only to changes in the basic airframe and controller logic and mechanization, but also to the displays used, types of inputs considered, and the dimensions of the approach window at the decision height. Therefore, competing airframes (such as B-747, DC-10, L-1011), competing control systems, or competing displays (e.g., flight directors) can be compared directly. The model has a further capability in that the effects of changes in the approach window can also be assessed easily.

Some final comments should be made regarding the use of the computed probabilities. First, these results must not be misinterpreted as providing an alternative to simulation and flight testing. Instead they should be considered

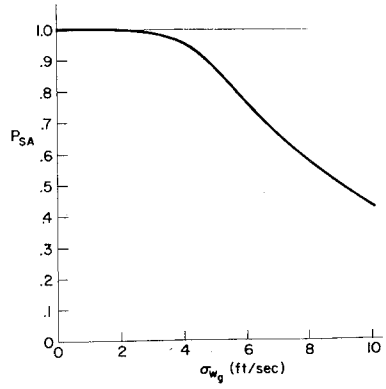

Fig. 11 Probability of a successful approach as a function of the w_g-gust intensity (System A).

Table 7 Closed-loop transfer functions for System C

$$\frac{d}{u_g} = \frac{-0.283(0)(2.0)(15.229)[0.134,2.087]}{(0.028)(2.066)(15.228)[0.445,0.465][0.206,2.039]}$$

$$\frac{d}{w_g} = \frac{-0.75(0.111)(2.0)(15.139)[0.291,1.76]}{(0.028)(2.066)(15.228)[0.445,0.465][0.206,2.039]}$$

$$\frac{d}{d_{\text{command}}} = \frac{-1.426(0.035)(-3.606)(4.396)}{(0.028)(2.066)(15.228)[0.445,0.465][0.206,2.039]}$$

$$\frac{u}{u_g} = \frac{0.0373(0.12)(1.35)(2.169)(15.228)[0.176,1.995]}{(0.028)(2.066)(15.228)[0.445,0.465][0.206,2.039]}$$

$$\frac{u}{w_g} = \frac{-0.136(2.051)(15.224)[-0.17,0.442][0.165,1.96]}{(0.028)(2.066)(15.228)[0.445,0.465][0.206,2.039]}$$

$$\frac{u}{d_{\text{command}}} = \frac{0.194(0)(4.03)(-4.082)}{(0.028)(2.066)(15.228)[0.445,0.465][0.206,2.039]}$$

as preliminary calculations, useful for such things as comparisons between competing systems. Second, the confidence level of the results is a direct function of the confidence level of the gust inputs. But because this information is not currently available, no estimate can yet be made for the confidence level of the computed probabilities.

Appendix: Summary of Numerical Constants for the Example Systems

This appendix consists of pertinent summary tables taken from Ref. 4. In addition, the longitudinal perturbation equations of motion are given in Eq. (13) for easy reference.

The example aircraft is a DC-8 defined by the landing approach parameters given in Table 4. Table 5 then follows with a list of the various control system constants that were shown in Figs. 3 and 4 (earlier). Finally, the closed-loop system transfer functions used in computing the pertinent rms values are given in Tables 6 and 7.

$$\begin{bmatrix} s - X_u & -X_w & g\cos\Theta_0 \\ -Z_u & s - Z_w & -U_0 s + g\sin\Theta_0 \\ -M_u & -(M_{\dot{w}}s + M_w) & s(s - M_q) \end{bmatrix} \begin{bmatrix} u \\ w \\ \theta \end{bmatrix} = \begin{bmatrix} X_{\delta_e} \\ Z_{\delta_e} \\ M_{\delta_e} \end{bmatrix} \delta_e \quad (13)$$

$$\dot{h} = -U_0\sin\Theta_0 - w\cos\Theta_0 + u\sin\Theta_0 + U_0\cos\Theta_0\theta$$

References

[1] Wood, K. A., "The Calculation of Weather Minima—Part I, RVR Minima," *All-Weather Operations Panel, Third Meeting, Vol. II, Selected Working Papers*, International Civil Aviation Organization Doc. 8685, AWOP/III-2, 1967, pp. 167–185.

[2] Chalk, C. R., T. P. Neal, T. M. Harris, F. E. Pritchard, and R. J. Woodcock, *Background Information and User Guide for MIL-F-8785B(ASG)*, "Military Specification—Flying Qualities of Piloted Airplanes," AFFDL-TR-69-72, Aug. 1969, Wright-Patterson Air Force Base, Ohio.

[3] Criteria for Approval of Category II Landing Weather Minima, FAA AC 120-20, June 6, 1966.

[4] Johnson, W. A., and D. T. McRuer, *Development of a Category II Approach System Model*, TR 182-3, Nov. 1970, Systems Technology, Inc., Hawthorne, Calif.

DECEMBER 1971 J. AIRCRAFT VOL. 8, NO. 12

Prediction of Installed Nozzle Flowfields

W. Presz Jr.,* M. Konarski,† and E. Grund‡

Pratt & Whitney Aircraft, East Hartford, Conn.

Spreiter and Alksne's method of local linearization was improved and used for inviscid-transonic-flow calculations over axisymmetric bodies of revolution (equivalent bodies). This solution was iteratively coupled with a boundary-layer inner solution allowing it to be used over bodies with slight slope discontinuities. The results of applying this method to simple axisymmetric fuselages and afterbody shapes are compared with experiments. For nonaxisymmetric bodies, cross-flow corrections are derived from incompressible flow theory and are coupled with the equivalent body results to approximate the complete transonic flowfield. The analysis is shown to be useful for supplementing test data and predicting installed nozzle performance.

Introduction

ONE of the most complex and demanding problems during the design of new aircraft is the proper integration of the propulsion system into the airplane structure. Here the aircraft/nozzle interface is of special importance, since the external flowfield set up by the vehicle exerts control over the aft-end flow, and hence, external pressure environment of the exhaust system. As a result, the thrust-minus-drag characteristics of the nozzle may change substantially and significantly affect vehicle performance. In addition, certain nozzle types (plug nozzles, blow-in-door ejectors) experience beneficial interactions between the external and internal flowfields to broaden the range of efficient nozzle operating conditions. In these cases, information about the flowfield external to the nozzle is even more critical.

Information on these interactions or installation effects is generated primarily by airframe/nozzle models in a wind tunnel. Wind-tunnel test data, however, are usually confined to measurements of gross aft-end forces to speed data recording and thereby, minimize the occupancy time required for these costly experiments. At best, only small amounts of pressure distribution data are measured making evaluation of

Presented as Paper 70-700 at the AIAA 6th Propulsion Joint Specialist Conference, San Diego, Calif., June 15–19, 1970; submitted July 16, 1970; revision received May 28, 1971.

* Senior Analytical Engineer, Inlets & Nozzles Group, Advanced Gas Turbines. Associate Member AIAA.

† Assistant Project Engineer, Inlets & Nozzles Group, Advanced Gas Turbines.

‡ Project Engineer, Inlets & Nozzles Group, Advanced Gas Turbines. Associate Member AIAA.